The Status and Physics Potential of the LHC

Peter Loch[1]

Department of Physics, University of Arizona, Tucson, Arizona 85721, USA

Abstract. The Large Hadron Collider (LHC) at the European center for high energy research (CERN) near Geneva, Switzerland, has been designed to collide protons with the highest center of mass energies ($\sqrt{s} = 14$ TeV) and luminosities (up to 10^{34} cm^{-2} s^{-1}) for any particle collider to date. The main physics goal at this accelerator and its two multi-purpose experiments ATLAS and CMS is the discovery of the Standard Model Higgs boson, which is expected within an integrated luminosity $\int \mathscr{L} dt = 10$ fb^{-1}, or the first three years of collisions, in the mass range of $115 - 180$ GeV. In addition, measurements of Standard Model parameters like the W boson mass m_W and top quark mass m_t are possible at high precision, with $\delta m_W \leq 15$ MeV and $\delta m_t \leq 1$ GeV. Illumination of new, yet unexplored kinematic domains in proton-proton collisions allows exploration of an enormous parameter space of new physics models beyond the Standard Model, including a possible early discovery of supersymmetry within $\int \mathscr{L} dt = 1$ fb^{-1}.

Keywords: LHC, detectors, Higgs searches, SUSY searches, mass spectroscopy top quark and W boson, jets
PACS: 29.20.db,29.40.Vj,29.40.Gx,12.38.Qk,13.85.-t,14.80.Bn,14.80.Ly

INTRODUCTION

The Large Hadron Collider (LHC), presently commissioned for first proton-proton (pp) collisions at CERN, Geneva, Switzerland, has been designed to collide protons at a center of mass energy of $\sqrt{s} = 14$ TeV, with a luminosity of $\mathscr{L} = 10^{34}\text{cm}^{-2}\text{s}^{-1}$. This makes it the highest energy and collision rate man-made particle collider so far. The physics potential of this machine, which can accelerate, store, and collide protons as well as heavy ions, reaches into yet unexplored kinematic domains with high expectations for detecting missing ingredients of the Standard Model, improving the precision on some of its parameters, determining parton density functions in the proton in these domains, and the discovery of new physics. In particular, the discovery of the elusive Higgs boson and thus the final experimental confirmation of this mass generating field suggested in the Standard Model and some of its extensions, is an important goal for the two multi-purpose experiments ATLAS and CMS installed in LHC.

In this article the physics potential of the LHC is reviewed. It starts with a brief look at the accelerator and its main parameters, followed by short descriptions of ATLAS and CMS. Then, selected predictions for Standard Model (SM) measurements are shown, and expectations for the discovery of the Higgs boson and strategies for its detection are discussed. The discovery potential for new physics beyond the Standard Model is presented for examples of searches for supersymmetry (SUSY). The article concludes with a brief status of the accelerator.

---

[1] presently visiting INFN Pisa, Pisa, Italy.

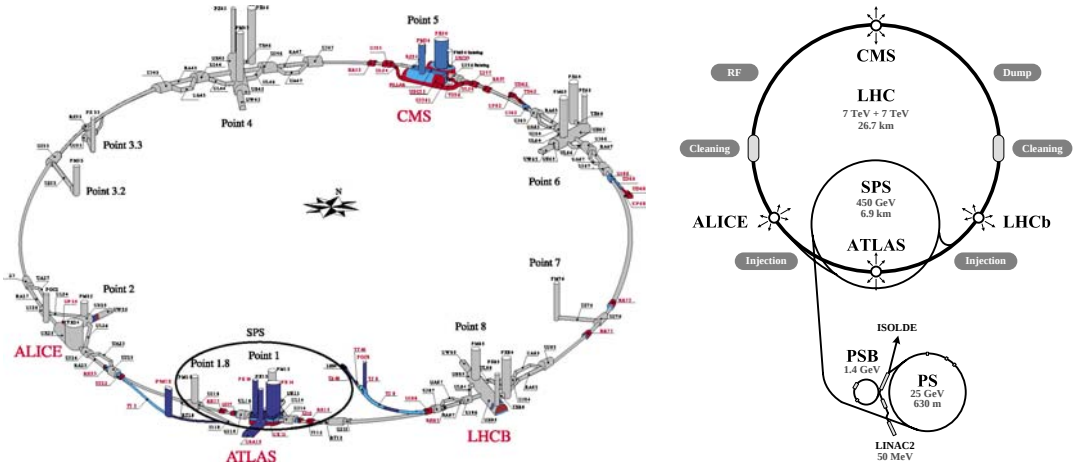

FIGURE 1. Schematics of Large Hadron Collider (LHC) and the proton accelerator complex at CERN.

THE LARGE HADRON COLLIDER

The LHC, as shown schematically in Fig. 1 and described in detail in Ref. [1], accelerates and stores protons in two beams circulating in opposite directions through the 26.7 km long tunnel which was already used for the Large Electron Positron collider (LEP) (e.g., see Ref. [2]), in operation from 1989 to 2000.

LHC utilizes a total of 1232 bending magnets and 392 focusing magnets to keep protons on the desired orbits, and to steer them to the interaction regions of the experiments. All magnets are superconducting, with a total of about 96 tons of liquid Helium stored in the ring to keep the operational temperatures around 1.9 K. The protons are injected into LHC with an energy of 450 GeV from the Super Proton Synchrotron (SPS), after several acceleration stages, starting with the linear accelerator LINAC2 (50 MeV), the Proton Synchrotron Booster PSB (1.4 GeV), and the Proton Synchrotron PS, which injects protons into SPS with 25 GeV (Fig. 1). In LHC the protons are accelerated to their final energy[2] of 7 TeV using two 400 MHz radio frequency (RF) cavities, one for each beam. A complete fill has 2808 bunches of approximately 1.2×10^{11} protons in each beam at design luminosity $\mathscr{L} = 10^{34}\text{cm}^{-2}\text{s}^{-1}$. The spacing between two bunches is about 7.5 m or 25 ns, see Ref. [1]. This means that the colliding beam experiments at LHC must accommodate bunch crossings at a rate of approximately 40 MHz. Taking the total pp cross-section σ_{pp} from Ref. [3] to be $\sigma_{pp} = \sigma_{pp}^{elast} + \sigma_{pp}^{inel} \approx 102$ mb, including $\sigma_{pp}^{elast} \approx 23$ mb for elastic scattering, the total inelastic pp cross-section σ_{pp}^{inel}, which includes single and double refractive collisions, is $\sigma_{pp}^{inel} \approx 79$ mb. This results in an average of about 20 (Poisson-distributed) inelastic pp collisions in a single bunchcrossing.

---

[2] Initial operation scenarios foresee first physics running at $\sqrt{s} = 10$ TeV (two 5 TeV beams). See `lhc-commissioning.web.cern.ch/lhc-commissioning` for actual schedules.

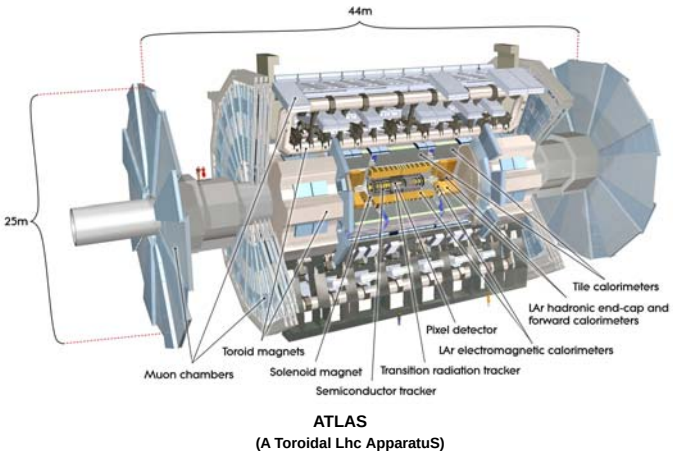

Overall length	≈ 46 m
Overall diameter	≈ 23 m
Overall weight	$\approx 7,000$ t
Solenoid field	2 T

FIGURE 2. The ATLAS detector at the LHC.

EXPERIMENTS AND EXPERIMENTAL CONDITIONS

Two of the six experiments at LHC employ large multi-purpose detector systems. ATLAS [4] and CMS [5] both feature near hermetic coverage for complete final state reconstruction around the LHC collision points Point 1 and Point 5, respectively (Fig. 1). The emphasis of the design of these two detectors is to allow precision reconstruction of all relevant final states in Standard Model and discovery physics in the high energetic *pp* collisions, but both are also adequate for reconstructing heavy ion collisions as well.

Two more specialized experiments, LHCb [6] for heavy flavour physics, especially in the *b*-quark sector and possible Standard Model extensions, and ALICE [7] for heavy ion collisions at yet unexplored temperatures, are located at Point 8 and Point 2, respectively. The physics potential of ALICE is summarized in Refs. [8, 9]. The two remaining smaller experiments also not further discussed here are dedicated to very forward (high pseudorapidity) physics, LHCf [10] and TOTEM [11].

The full physics potential of ATLAS, based on the evaluation of detailed detector simulations of a long list of predicted processes from the Standard Model, including the SM Higgs sector, and beyond the Standard Model, the latter including SUSY extensions and exotic processes, can be found in Ref. [12]. A similar collection of physics performance evaluations is available for CMS in Refs. [13, 14].

ATLAS and CMS at the LHC

Both ATLAS and CMS follow a similar basic design with an inner tracking detector surrounded by electromagnetic and hadronic calorimetry, which in turn is surrounded by a muon spectrometer. The main differences are the magnetic field and the arrangements of the magnets. ATLAS has a solenoid field of about 2 T in its inner cavity for precision $r-\phi$ tracking and vertex reconstruction, and a toroidal field of varying strength for the muon detector, which allows high precision reconstruction of all momentum com-

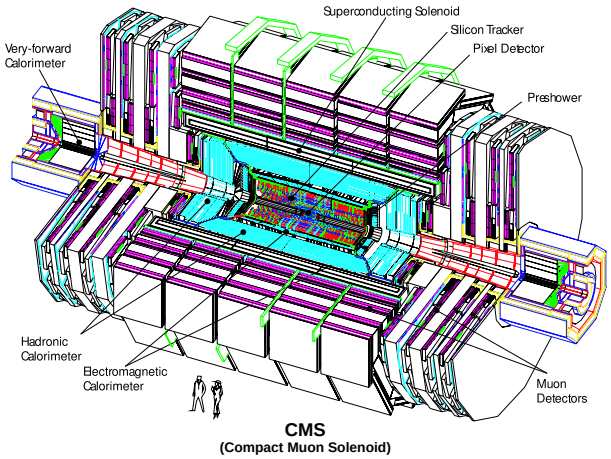

Overall length	≈ 22 m
Overall diameter	≈ 15 m
Overall weight ...	$\approx 12,500$ t
Solednoid field	4 T

FIGURE 3. The CMS detector at the LHC.

ponents. The solenoid magnet is located in front of the calorimeter system, while the air core toroid surrounds the whole experiment, see Fig. 2. CMS features a solenoid magnet with a 4 T field, with the magnet encompassing the calorimeters and the muon spectrometer surrounding it, see Fig. 3.

The two experiments employ very different calorimeter technologies, with CMS featuring a highly granular lead-tungstate ($PbWO_4$) crystal calorimeter for electromagnetic and a tiled scintillator/brass calorimeter for hadronic calorimetry. ATLAS, on the other hand, has liquid argon with lead and copper absorbers for electromagnetic and hadronic calorimetry, respectively, and a tiled scintillator/iron hadronic calorimeter in the central region. Both calorimeter systems have a highly granular lateral readout structure, with up to seven(three) depth segments in ATLAS(CMS). In case of ATLAS this granularity leads to nearly $200,000$ readout channels for the calorimeters alone.

Both detector systems allow reconstructing particles with high efficiency and precision. Typical parameters are a 90% reconstruction efficiency for $\mu^{\pm}$ and 80% for $e^{\pm}$, both with rejection of the most severe background from (light quark) jets at a level of 10^5. Photons can be reconstructed with about 80% efficiency, but at a lower jet rejection of typically 10^3. b-jets and $\tau^{\pm}$ are reconstructed with $50-60$% efficiencies and a jet rejection of about 100. It should be noted that, as both experiments feature different detector technologies, especially concerning calorimetry, efficiencies and purities differ in details.

ATLAS and CMS each provide hermetic coverage in azimuth $0 \leq \phi < 2\pi$ and within pseudorapidities of $|\eta| < 5$. This is particularly important for the precision reconstruction of the missing transverse momentum generated by neutrinos and other non-interacting particles in the final state of the pp collisions. Both experiments employ very precise tracking, calorimeters and muon spectrometers, to measure electron and photon energies with a high energy limit in the relative energy resolution of less than 1%, and the muon momentum within fluctuations of typically a few percent, with a sufficient relative transverse momentum resolution around 10% for muons with $p_T = 1$ TeV. Jets are reconstructed with high efficiency, typically more than $90(95)$% for jets with $p_T > 60(100)$ GeV, and a sufficient relative energy resolution with a high energy limit

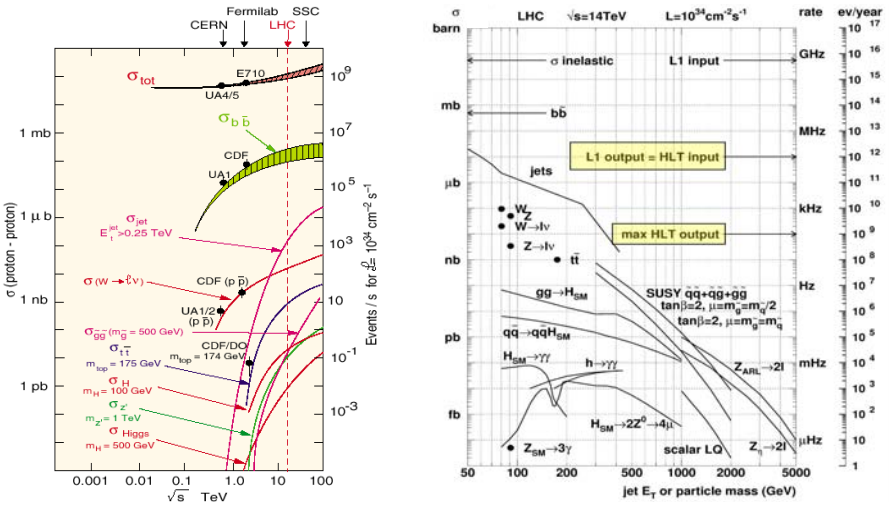

FIGURE 4. Total and process cross-sections in pp and $p\bar{p}$ collisions, as function of the center of mass energy $\sqrt{s}$ (left). The event rate at LHC design luminosity $\mathscr{L} = 10^{34}\text{cm}^{-2}\text{s}^{-1}$ is given on the right scale of this graph. The plot on the right shows the rates expected at $\sqrt{s} = 14$ TeV and design luminosity, as function of the jet transverse energy or particle mass. Indicated are the cross-sections (right scale) as well as the event rate per year (left scale).

in the order of a few percent.

Trigger and background issues

One of the most important tasks for each experiment is to reduce the high interaction rate to a manageable event rate, i.e. the rate at which the data can be recorded (typically up to 200 Hz). As the left plot in Fig. 4 indicates, the total cross-section is dominated by SM processes driven by strong interactions (QCD). All cross-sections of interest, especially the ones for discovery physics including Higgs production and new physics, are orders of magnitude smaller. In particular in the Higgs mass range between 100 and 300 GeV, which is of highest interest for discovery, jet production from QCD dominates, see right plot in Fig. 4.

The task of the event triggers and online event filters is to enhance the events of interest in the recorded sample by suppressing the less interesting signatures. This is realized by a three level trigger system, where the first level trigger[3] (L1) reduces the event rate from 40 MHz down to about 75 kHz in less than 2 μs, based on a fast search for so-called regions of interest (RoI), i.e. regions with significant signal in the calorimeters and the muon spectrometers. L1 also performs a fast analysis of the RoI signal itself for a first attempt to classify its source ($e^{\pm}/\gamma$, $\mu^{\pm}$, $\tau^{\pm}$, and jets). Some simple combinations of RoI signals, focusing on specific topologies of the final states of interest, are considered in the L1 decision as well as rough estimates for missing transverse energy.

[3] All numbers and strategies discussed here are for the ATLAS experiment, but similar for CMS.

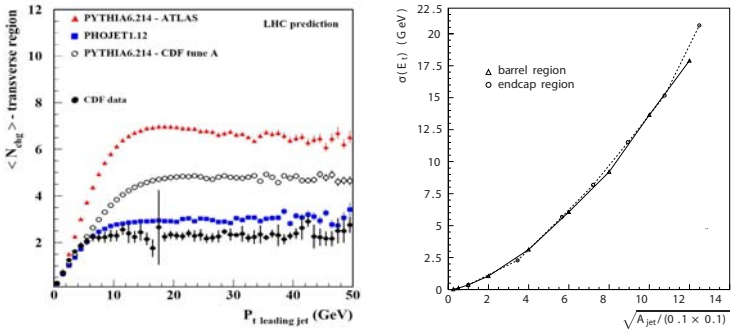

FIGURE 5. The left figure shows the average number of charged tracks in the regions away from the jets in QCD di-jet production, as function of the hardest jet p_T. Experimental data is from CDF [15], LHC estimates are from Ref. [17]. The figure on the right shows the expected fluctuation in the transverse momentum measurement as function of the jet area, for two different regions of the ATLAS detector (both figures extracted from Ref. [18]).

The events accepted by L1 are analyzed in more detail by the second level trigger L2, which now includes tracks from the inner detectors. L2 reduces the event rate further to about 1 kHz, within a decision time of less than 10 ms. Events accepted by L2 are handed to the event filter (EF), where the full event data is available and slightly adapted precision offline algorithms are run to make a final selection on event topologies of interest. The final EF output rate is up to 200 Hz, and its decision time is 1 s. The events passing the EF are recorded and fully reconstructed offline.

The *pp* collision at LHC have intrinsic background contributions which are potential sources of additional signal fluctuations (noise), and signal (extra energies associated with a reconstructed particle or jet), or topology biases, e.g. extra jets not belonging to the hard scattering of interest. First, the underlying event (UE), already well studied at the Tevatron [15, 16], are collisions of other partons in the same two protons generating the hard scattering process. The second contribution are multiple interactions (MI), i.e. collisions of partons in other protons in the same bunch crossing.

The UE activity, yet unknown at LHC, can be evaluated by analyzing the transverse energy flow away from the two (back-to-back) jets in QCD di-jet production, as suggested in Ref. [15]. Estimates of this transverse energy flow in ATLAS, derived from calculations documented in Ref. [17], are shown in the left plot of Fig. 5.

Multiple interactions potentially generate a signal baseline and a signal history, i.e. signal fragments from previous and even the following bunch crossing affect the actual signal, mainly due to the relatively slow readout of the calorimeters, compared to the 25 ns bunch crossing time. The size and qualitative effect on the signal of interest at a given luminosity depends on the readout electronics, especially the analog signal shaping, which is designed to minimize these signal biases as much as possible. Typically the overall effect is limited to increased signal fluctuations with only a small amount of additional signal, as discussed in Ref. [4] for ATLAS and Ref. [14] for various physics channels in CMS. For example, the right plot in Fig. 5 shows these fluctuations in the transverse momentum measurement as function of the jet area, both in the central and more forward regions of ATLAS (original calculations in Refs. [19, 20]).

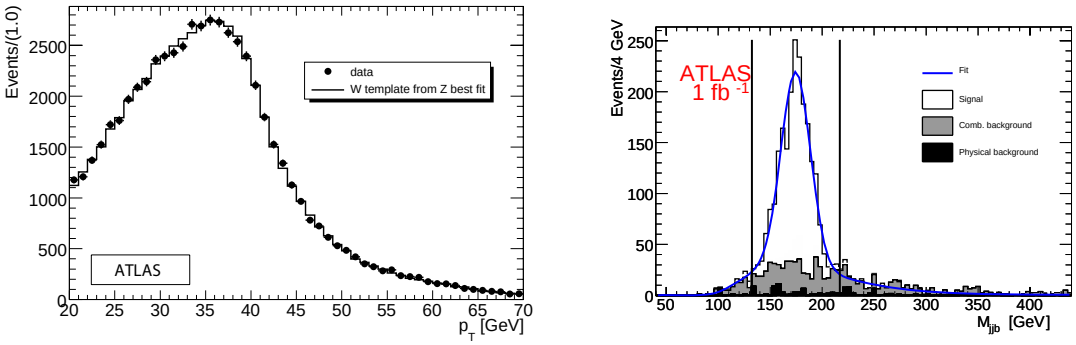

FIGURE 6. The p_T spectrum of muons from $W \to \mu\nu_\mu$ decays (left). The points indicate expectations for data from full (detailed) simulations for ATLAS, while the histogram shows the true $\mu\ p_T$ distribution derived with templates from Z-boson decays. The right plot shows the invariant mass reconstructed from full hadronically decaying top quarks ($t \to Wb \to jjb$) together with the background in ATLAS. Both figures have been extracted from Ref. [12].

The initial experimental conditions at LHC are likely characterized by a lower luminosity of $\mathscr{L} \approx 10^{32}\text{cm}^{-2}\text{s}^{-1}$, a different bunch crossing rate (75 ns, about 13 MHz), and different proton beam energies (5 TeV), all of which affect the MI contributions to the signal. The first important measurements are therefore the transverse energy flow and charged track distributions in minimum bias collisions at various luminosities, within the (different) acceptance limitations introduced by ATLAS and CMS. These measurements then allow tuning of the soft, non-perturbative QCD physics in the generator models, which drives most of the MI dynamics. This excercise, together with the measurements of the UE activity discussed above, is essential to unfold the corresponding signal contributions in any precision physics analysis at LHC.

STANDARD MODEL PHYSICS AT LHC

One of the first aspects of hard scattering physics at LHC to be measured are SM cross-sections in the new and fairly extended kinematic domain, as those are important backgrounds for discovery physics. In particular, light quark jet production in QCD and heavy quark final states like $t\bar{t}$ pairs need to be understood and controlled not only for SM Higgs searches, but also for possible SUSY and other new physics beyond the SM (BSM) discoveries. The event rate for SM processes is high even at lower luminosity. For example, with only 1 fb^{-1} of collected data, which corresponds to about one year of data taking at a possible initial $\mathscr{L} = 10^{32}\text{cm}^{-2}\text{s}^{-1}$, one can expect more than $100,000$ jets with $p_T > 1$ TeV. The reconstruction quality of many final state physics objects is therefore quickly dominated by systematic rather than statistical uncertainties. This means that systematics need to be evaluated and addressed early on, as they introduce severe limitations on the precision measurement of SM cross-sections, and therefore the determination and experimental validation of parton density functions for the proton in kinematic domains not yet covered by other experiments. These measurements are important for controlling the background in Higgs, SUSY, and BSM searches, and thus

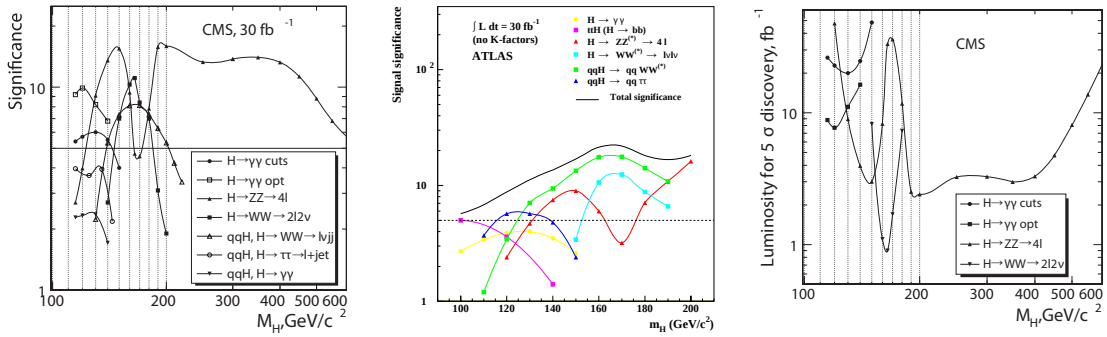

FIGURE 7. Significance of the Standard Model Higgs signal in various decay modes at 30 fb $^{-1}$ of collected data, as function of the Higgs mass m_H, for CMS (left, Ref. [14]) and for the lower mass range in ATLAS (center, Ref. [21]). The plot on the right shows the integrated luminosity needed for a 5σ discovery of the Standard Model Higgs for three different decay modes, as function of m_H (Ref. [14]).

for the cross-section measurements for the corresponding new processes themselves.

Precision measurements of the W-boson (m_W) and the top quark masses (m_t) are expected to be possible with uncertainties of $\delta m_W \leq 15$ MeV and $\delta m_t \leq 1$ GeV. Figure 6 (left) indicates that the distribution of the p_T of the μ from the leptonic $W \to \mu\nu_\mu$ decay can be used to constrain m_W in a fit using kinematic distribution templates derived from $Z \to \mu^+\mu^-$ decays, even within a low $\int \mathscr{L} dt = 15$ pb^{-1}, where the statistical and systematic uncertainties of this measurement are estimated to be of about the same size in ATLAS, $\delta m_W \approx 120$ MeV (details in Ref. [12]).

The top quark reconstruction in $t\bar{t}$ events is expected to be possible with an initial systematic uncertainty of $\delta m_t \approx 1-3.5$ GeV for the fully hadronic top quark decay $t \to Wb \to q\bar{q}b$ at $\int \mathscr{L} dt = 1$ fb^{-1}, under the assumption of a systematic jet energy scale error between $1-5\%$. As the hadronic decay of the W bosons in these events can be used to control the light quark jet energy scale, the main uncertainty comes from the b-quark jet energy scale. The statistical error is already considerably smaller (around 0.4 GeV) at this integrated luminosity. All these numbers are expected for ATLAS, see Ref. [12]. Figure 6 shows on the right the top mass spectrum for the hadronic top decays with two light quark jets and one tagged b-jet.

STANDARD MODEL HIGGS DISCOVERY POTENTIAL

The main goal of the LHC physics program, the discovery of the (Standard Model) Higgs boson, presents significant experimental challenges to both ATLAS and CMS. A summary of the theoretical aspects of Higgs production at LHC are presented in Ref. [22]. The paramount experimental challenge for Higgs searches lies in the suppression of the typically large background from QCD and electroweak decays, especially generated by topologies like $t\bar{t}$, and the (related) limitations on the precision of the Higgs mass (m_H) measurement. The presently considered range for m_H is given by the combined results of the four LEP experiments, experimentally excluding $m_H < 114.4$ GeV at the 95% confidence level, see the summary in Ref. [23]. The theoretical upper limit

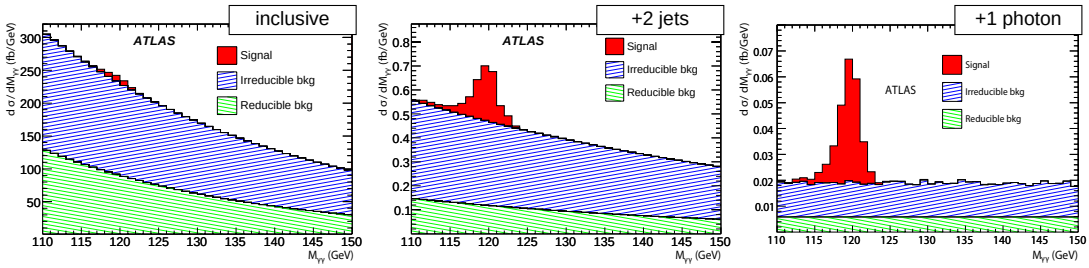

FIGURE 8. The inclusive $H \to \gamma\gamma$ invariant mass cross-section on top of the reducible and irreducible background (left). The exclusive cross-sections for the $\gamma\gamma$ final state plus two additional jets and $\gamma\gamma$ plus one additional photon are shown in the center and right plots, respectively (adapted from Ref. [12]).

at the TeV scale is around 700 GeV (Ref. [24], for example). Global fits to all relevant Standard Model parameters from LEP (e.g. electroweak parameters) and Tevatron (top mass) indicate an experimentally preferred upper limit[4] of 185 GeV [26].

Figure 7 left and center show the significance of the Higgs signal in various decay modes for CMS and ATLAS as function of m_H, at $\int \mathscr{L} dt = 30$ fb^{-1}, or after about three years of data taking at 10^{33}cm^{-2}s^{-1}. The different sensitivities in both experiments to certain decays are due to the different detector technologies and the corresponding differences in signal reconstruction quality and resolution, as well as the different acceptances for the specific ingredients of the decay mode and backgrounds. Exclusions of some these final states is expected to be possible within a few 100 pb^{-1} of collected data. Discovery of a heavier Higgs boson with $160 < m_H < 180$ GeV is possible within $\int \mathscr{L} dt = 1$ fb^{-1}, while a few 10 fb^{-1} should allow to cover the full m_H range, see the integrated luminosity needed for discovery as function of the m_H for $H \to \gamma\gamma$, $H \to ZZ \to 4\ell$, and $H \to WW \to 2\ell 2\nu$ for CMS in Fig. 7 (right).

For lower m_H the $H \to \gamma\gamma$ decay is one of the important modes for discovery, in particular for CMS. For ATLAS this final state alone is not significant enough for discovery in the relevant range of m_H. A combined search for this and the $H \to \tau\tau$ signature, for example, is expected to increase the significance of the signal considerably, especially when tagging the associated (forward) jets in vector boson fusion (VBF) generated Higgs, as can be seen from the center plot in the same Fig. 7.

The inclusive invariant mass spectrum of the $\gamma\gamma$ final state is dominated by background, see Fig. 8. This figure also shows that the Higgs signal significance can be considerably larger in several exclusive final states including the $H \to \gamma\gamma$ decay, like when associated with one or two additional jets or one extra photon. Statistical combination of the significances of the most relevant of these channels increases the total Higgs signal-to-background ratio compared to the inclusive analysis with acceptable loss of overall statistics, as evaluated in more detail in Refs. [12, 14].

The "golden channel" for Higgs discovery, even at lower m_H, is the $H \to ZZ^* \to 4\ell$ final state, because the precision reconstruction of the charged leptons is very efficient, and the backgrounds are small and controllable, see left plot in Fig. 9 for $m_H = 130$ GeV

[4] Tevatron recently excluded $m_H = 170$ GeV at a confidence level of 95% , see Ref. [25].

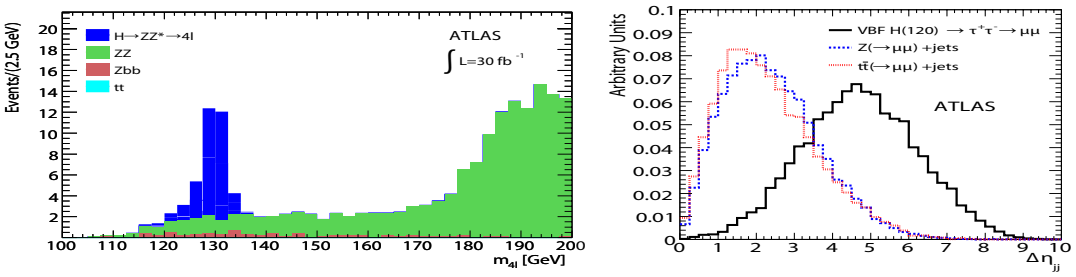

FIGURE 9. The $H \to ZZ^* \to 4\ell$ signal on top of the most important backgrounds, for $m_H = 130$ GeV and an integrated luminosity of 30 fb^{-1} (left). The right figure shows the distance $\Delta\eta_{jj}$ between the two hardest jets in VBF Higgs production and in relevant backgrounds (both plots from Ref. [12]).

in ATLAS. The right plot in this figure shows an example for the characteristic topology in VBF produced Higgs, which represent a few percent of the total production cross-section in the lower mass range (e.g., see Ref. [27] for a full review). In this production mode the two quarks radiating off the W bosons in $qq \to qqWW \to qqH$ give rise to two forward going "tag" jets. These jets are widely separated in η and thus lead to a very distinct event topology when compared to the most relevant decay backgrounds.

PHYSICS BEYOND THE STANDARD MODEL

Theoretical and phenomenological aspects of new particle production at LHC are summarized elsewhere in these proceedings [28]. For a full overview of the physics potential for discovery of new physics, including supersymmetric Higgs bosons and new exotic particles, of ATLAS and CMS, see Refs. [12, 14]. Here two examples for sensitive variables and topologies from SUSY models, accessible experimentally early on at LHC (1 fb^{-1}), are presented.

One of the important indications for the discovery of SUSY are possible final states including the lightest postulated SUSY particle (LSP), the neutralino $\tilde{\chi}_1^0$. Characteristic for these states are long decay chains with several leptons, jets, and considerable missing transverse energy in the final state, (Fig. 10).

Among the sensitive experimental variables for LSP discovery are the effective mass M_{eff} [29], which is the scalar sum of the p_T of the four hardest jets within $|\eta| < 2.5$, the p_T of all identified leptons, and the reconstructed missing transverse momentum. Figure 10 shows the M_{eff} spectrum for a given point in SUSY parameter space (SU3, bulk region[5]) and the relevant backgrounds in a zero-lepton inclusive search, after all selections.

An exclusive search for opposite sign charge, same flavour lepton pairs produced together with jets and missing transverse momentum generates the di-lepton mass spectrum shown on the left in Fig. 10. This mode is particularly attractive because of the small SM background and the sensitivity of the spectrum endpoint to mass ratios of slep-

[5] Model parameter settings at this point: $m_0 = 0$, $m_{1/2} = 300$ GeV, $A_0 = -300$ GeV, $\tan\beta = 6$, $\mu > 0$.

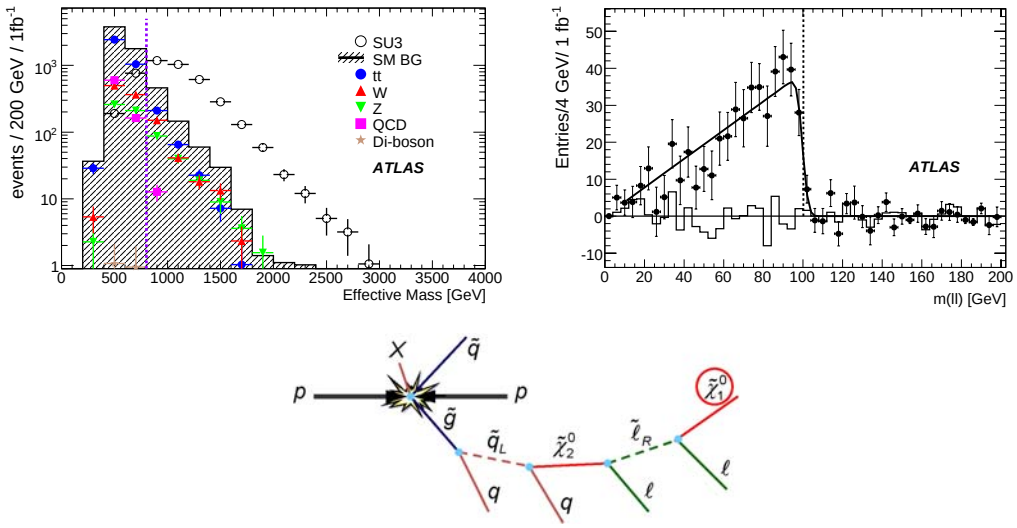

FIGURE 10. A typical LSP decay chain in SUSY (bottom). Among the experimental sensitive variables are M_{eff}, see spectrum in the top left plot for an the inclusive zero-lepton search at SU3, and the cutoff point in the opposite sign charge, same flavour di-lepton pair mass $M_{\ell\ell}$ spectrum in an exclusive search (top right). All spectra are obtained after all other kinematic selections, see Ref. [12].

tons and the two lightest neutralinos in decays like $\tilde{\chi}_2^0 \to \tilde{\ell}^{\pm}\ell^{\mp} \to \ell^+\ell^-$. Other SUSY particle mass relations are accessible by measuring invariant masses between a final state quark (jet) and one or two of the lepton(s).

SUMMARY

The physics potential of the *pp* collisions at the LHC has been evaluated by the ATLAS and CMS experiments using a multitude of SM and new physics processes and detailed detector simulations. From these studies the discovery of the SM Higgs boson in the most relevant mass range $115 < m_H < 180$ GeV is predicted within $\int \mathscr{L} dt = 30$ fb^{-1}, i.e. about three years of data taking at an initially lower than design luminosity of $\mathscr{L} = 10^{33}$cm^{-2}s^{-1}. SUSY, if existing, may manifest itself even earlier. First evidence and even discovery of the corresponding particles can be expected within $\int \mathscr{L} dt = 1$ fb^{-1}, at least in some regions of the SUSY parameter space. High precision Standard Model physics, like measuring the W boson or top quark mass, can already be feasible at even lower statistics (around 100 pb^{-1}), depending on the level of systematic uncertainties in the jet energy scale, for example.

The LHC first circulated single beams at 450 GeV on September 10, 2008 [30]. After a significant technical problem [31] the accelerator had to be turned off again on September 19, 2008, before first collisions could be facilitated. It is now planned to start LHC operations again by end of summer 2009 [32].

ACKNOWLEDGMENTS

First, I like to acknowledge the LHC community, including the experiments, for the enormous work they have performed to develop the extensive expectations for the physics potential at this machine. I also like to thank the organizers of the XIII Mexican School of Particles and Fields, here in particular A. Ayala and M.E. Tejeda-Yeomans, for the opportunity to report on the subjects in this article, and the excellent organization of this conference. Last but not least I like to thank the funding agencies, in particular the US Department of Energy and the INFN Italy, for their continuing support.

REFERENCES

1. L. Evans, and P. Bryant, *JINST* **3**, S08001 (2008).
2. E. Picasso, and G. Plass, *Europhys. News* **20**, 80–91 (1989).
3. C. Amsler, et al., *Phys. Lett.* **B667**, 1 (2008).
4. G. Aad, et al., *JINST* **3**, S08003 (2008).
5. R. Adolphi, et al., *JINST* **3**, S08004 (2008).
6. A. A. Alves, et al., *JINST* **3**, S08005 (2008).
7. K. Aamodt, et al., *JINST* **3**, S08002 (2008).
8. F. Carminati, et al., *J. Phys.* **G30**, 1517–1763 (2004).
9. B. Alessandro, et al., *J. Phys.* **G32**, 1295–2040 (2006).
10. O. Adriani, et al., *JINST* **3**, S08006 (2008).
11. G. Anelli, et al., *JINST* **3**, S08007 (2008).
12. G. Aad, et al. (2009), CERN-OPEN-2008-020.
13. G. L. Bayatian, et al. (2006), CERN-LHCC-2006-001.
14. G. L. Bayatian, et al., *J. Phys.* **G34**, 995–1579 (2007).
15. A. A. Affolder, et al., *Phys. Rev.* **D65**, 092002 (2002).
16. D. E. Acosta, et al., *Phys. Rev.* **D70**, 072002 (2004).
17. A. Moraes, C. Buttar, and D. Clements, Measuring the underlying event at atlas, Tech. Rep. ATL-PHYS-PUB-2005-015. CERN-ATL-PHYS-PUB-2005-015, CERN, Geneva (2005).
18. S. Ellis, J. Huston, K. Hatakeyama, P. Loch, and M. Tonnesmann, *Prog. Part. Nucl. Phys.* **60**, 484–551 (2008).
19. R. Davis, and P. Savard, A study of pileup noise in the barrel and endcap calorimetry, Tech. Rep. ATL-CAL-96-084. ATL-AC-PN-84, CERN, Geneva (1996).
20. P. Savard, and G. Azuelos, *Potentiel De Decouverte D'un Boson De Higgs Lourd Avec Le Detecteur Atlas*, Ph.D. thesis, Montréal Univ., Montréal (1998), UMI-ND35637 (in french).
21. S. Asai, et al., *Eur. Phys. J.* **C32S2**, 19–54 (2004).
22. S. Dawson these proceedings.
23. R. Barate, et al., *Phys. Lett.* **B565**, 61–75 (2003).
24. M. Spira, and P. M. Zerwas (1997), hep-ph/9803257.
25. G. Bernardi, et al., Combined CDF and D0 Upper Limits on Standard Model Higgs Boson Production at High Mass $(155-200\ \mathrm{GeV}/c^{2})$ with 3 fb^{-1} of data, Tech. Rep. arXiv:0808.0534 (2008).
26. J. Alcaraz, et al., Precision Electroweak Measurements and Constraints on the Standard Model, Tech. Rep. arXiv:0712.0929. ALEPH-2007-001-PHYSICS-2007-001. CERN-PH-EP-2007-039. DELPHI-2007-002-PHYS-949. L3-Note-2834. LEPEWWG-2007-01. OPAL-PR-426, CERN, Geneva (2007).
27. A. Djouadi, *Phys. Rept.* **457**, 1–216 (2008).
28. M. Peskins these proceedings.
29. D. R. Tovey, *Eur. Phys. J. direct* **C4**, N4 (2002).
30. CERN Press Release PR08.08 (2008).
31. CERN Press Release PR14.08 (2008).
32. CERN Press Release PR17.08 (2008).